

Dissipation in relativistic pair-plasma reconnection

Michael Hesse and Seiji Zenitani

NASA Goddard Space Flight Center, Greenbelt, Maryland 20771, USA

(Received 12 July 2007; accepted 2 October 2007; published online 9 November 2007)

An investigation into the relativistic dissipation in magnetic reconnection is presented. The investigated system consists of an electron-positron plasma. A relativistic generalization of Ohm's law is derived. A set of numerical simulations is analyzed, composed of runs with and without guide magnetic field, and of runs with different species temperatures. The calculations indicate that the thermal inertia-based dissipation process survives in relativistic plasmas. For antiparallel reconnection, it is found that the pressure tensor divergence remains the sole contributor to the reconnection electric field, whereas relativistic guide field reconnection exhibits a similarly important role of the bulk inertia terms. © 2007 American Institute of Physics.

[DOI: 10.1063/1.2801482]

I. INTRODUCTION

Magnetic reconnection provides an effective means to effect plasma transport across the magnetic field and across magnetic topological boundaries in plasmas, for which the idealness condition

$$\vec{E} + \vec{v}_s \times \vec{B} = 0 \quad (1)$$

for each relevant plasma species s is violated somewhere in the domain under consideration.¹ Equation (1) can be interpreted as an expression for the electric field \vec{E} in terms of the bulk velocity \vec{v}_s and of the magnetic field \vec{B} . The key question addressed in many recent studies has been which processes are likely to supply additional electric field terms so that condition (1) is violated and reconnection may take place.

In a nonrelativistic, collisionless plasma, all possible terms can be derived from the electron momentum equation. Without any temporal or spatial averaging, the most general, nonrelativistic form of the electric field equation is

$$\vec{E} = -\vec{v}_e \times \vec{B} - \frac{1}{n_e e} \nabla \cdot \vec{\mathbf{P}}_e - \frac{m_e}{e} \left(\frac{\partial \vec{v}_e}{\partial t} + \vec{v}_e \cdot \nabla \vec{v}_e \right). \quad (2)$$

Candidate mechanisms for reconnection electric fields thus involve pressure-based effects, or bulk inertia effects, which are related to the velocity derivatives in Eq. (2). It should be noted that all of the last three terms result from the inertia of individual particles. The pressure-tensor divergence describes the inertial effects of the thermal particle motion, whereas the bulk inertia terms can be understood as the inertia associated with the motion of the center of mass of the electron distribution.²

Although some questions remain in turbulent plasmas, most recent investigations have found that, in the central magnetic reconnection region, the relevant additional term is provided by the thermal inertia.²⁻¹⁰ The physics behind this is associated with the transient nature of particle orbits in the reconnection region. Pre-acceleration particles are continuously transported into the reconnection region, whereas accelerated particles tend to leave. The role of the reconnection

electric field is to provide sufficient force to maintain a temporally constant or slowly varying current density.² Alternatively, one might consider the reconnection electric field to be maintained by displacement current effects, which appear whenever the current density reduces by the loss of accelerated particles. This scenario was found to hold regardless of the presence of a guide magnetic field.

Over the last few years, it has been realized the reconnection may also play a key role in astrophysical plasmas. Examples include coronal flares¹¹ or extra galactic jets¹² in active galactic nuclei (AGN), magnetic dissipation engine in pulsar winds,¹³⁻¹⁵ and probably also in gamma ray bursts.^{16,17}

Accordingly, the question how reconnection works in such plasma becomes relevant. In the absence of collisions, it is conceivable that relativistic effects may enhance bulk inertia effects to the point where they dominate the reconnection electric field. Therefore, the question of how the frozen-in condition is violated may have a different answer in a relativistic plasma. This question is the focus of the present paper. For simplicity, and since such plasmas are deemed relevant in astrophysical systems, we will study electron-positron pair plasmas. Although previous simulation works shed light on the relativistic particle acceleration,¹⁸⁻²² the main physics of the relativistic reconnection process is poorly understood.

A very successful first step toward shedding light on the relativistic reconnection process was recently undertaken by Bessho and Bhattacharjee.¹⁸ These authors found that reconnection proceeds at fast rates even in an electron-positron plasma, where Hall effects are absent. They verified that guide field reconnection tends to reduce the reconnection rate also in a relativistic plasma, and they agreed with previous studies^{19,21} that the reconnection electric field is a strong particle accelerator in relativistic plasmas.

Before embarking on the application of a numerical model, we will have to derive the relativistic generalization of Eq. (2). We will undertake the derivation of the basic equation set in Sec. II. Section III will introduce the numerical model, and the suite of modeled systems, and Sec. IV

will present a detailed analysis of the simulation results. Finally, Sec. V will present a summary and conclusions.

II. RELATIVISTIC FLUID EQUATIONS

Our approach to derive an electric field equation follows that of Taub²³ and of Wright and Hadley.²⁴ In a relativistic plasma, it is convenient to express distribution functions in terms of the momentum vector $\vec{u} = \gamma \vec{v}$, where

$$\gamma = \left(1 - \frac{v^2}{c^2}\right)^{-1/2} = \left(1 + \frac{u^2}{c^2}\right)^{1/2}. \quad (3)$$

With the relativistic particle equations of motion

$$\frac{d\vec{u}}{dt} = \frac{q}{m} (\vec{E} + \vec{v} \times \vec{B}), \quad (4)$$

$$\frac{d\vec{r}}{dt} = \vec{v}, \quad (5)$$

the relativistic generalization of the Vlasov equation has these orbits as its characteristics:

$$\frac{\partial f}{\partial t} + \frac{\vec{u}}{\gamma} \cdot \nabla f + \frac{q}{m} \left(\vec{E} + \frac{\vec{u}}{\gamma} \times \vec{B} \right) \cdot \frac{\partial f}{\partial \vec{u}} = 0 \quad (6)$$

with $f = f(\vec{r}, \vec{u}, t)$. Moment equations are derived in a standard manner by multiplying Eq. (6) by powers of \vec{u} and integration over \vec{u} space.

The continuity equation is thus

$$\frac{\partial}{\partial t} \int d^3u f + \nabla \cdot \int d^3u \frac{\vec{u}}{\gamma} f = 0, \quad (7)$$

which leads to the definitions

$$n = \int d^3u f \quad (8)$$

and

$$n \langle \vec{v} \rangle = \int d^3u \frac{\vec{u}}{\gamma} f. \quad (9)$$

The raw form of the momentum equation results from multiplication by the dyad $\vec{u}\vec{u}$ and by integration. A small amount of algebra leads to

$$\begin{aligned} m \frac{\partial}{\partial t} \int d^3u \vec{u} f + m \nabla \cdot \int d^3u \frac{\vec{u}\vec{u}}{\gamma} f - q E_k \int d^3u f \\ - q \int d^3u \frac{1}{\gamma} \vec{u} \times \vec{B} f = 0. \end{aligned} \quad (10)$$

With the definition

$$n \langle \vec{u} \rangle = \int d^3u \vec{u} f, \quad (11)$$

the raw momentum equation can be written as

$$m \frac{\partial}{\partial t} (n \langle \vec{u} \rangle) + m \nabla \cdot \int d^3u \frac{\vec{u}\vec{u}}{\gamma} f - q n (\vec{E} + \langle \vec{v} \rangle \times \vec{B}) = 0. \quad (12)$$

This equation could be solved for the electric field to yield a form similar to Eq. (2). However, it lacks a separation between bulk and thermal inertia effects. In analogy to the nonrelativistic case, we wish to obtain an inertial term of the form

$$m n \frac{\partial}{\partial t} \langle \vec{u} \rangle + m n \langle \vec{v} \rangle \cdot \nabla \langle \vec{u} \rangle = \dots \quad (13)$$

The combination of these two terms describes the temporal and convective changes of the average particle momentum. Expanding Eq. (12) leads then to

$$\begin{aligned} m n \left(\frac{\partial}{\partial t} \langle \vec{u} \rangle + \langle \vec{v} \rangle \cdot \nabla \langle \vec{u} \rangle \right) + m \nabla \cdot \left(\int d^3u \frac{\vec{u}\vec{u}}{\gamma} f - n \langle \vec{v} \rangle \langle \vec{u} \rangle \right) \\ - q n (\vec{E} + \langle \vec{v} \rangle \times \vec{B}) = 0, \end{aligned} \quad (14)$$

which suggests the definition

$$\vec{\mathbf{P}} = \int d^3u \frac{\vec{u}\vec{u}}{\gamma} f - n \langle \vec{v} \rangle \langle \vec{u} \rangle \quad (15)$$

for the pressure tensor. Although close in form to the nonrelativistic variant, the relativistic pressure tensor differs in one important aspect: symmetry. This property has important consequences and it deserves some discussion.

While momentum and velocity in a nonrelativistic plasma are described by the same (velocity) vector, this is no longer so in a relativistic plasma. In a relativistic plasma, however, the momentum flux $n \langle \vec{u} \rangle$ may have a different direction from the number flux $n \langle \vec{v} \rangle$; in fact, a distribution is easily constructed that has these two quantities opposing each other. The pressure tensor is a representation of the thermal momentum transport. The transport of the average momentum $n \langle \vec{u} \rangle$ is by the average velocity $n \langle \vec{v} \rangle$. The pressure tensor will exhibit a similar asymmetry.

There is one further important distinction to be considered. In a nonrelativistic plasma, the pressure tensor is invariant (except for rotation) under a Galilei transformation. It is quite obvious that its relativistic generalization cannot be invariant under Lorentz transformation since the location of the center of momentum of a distribution depends heavily on how many particles are moving close to the speed of light. Therefore, the separation of inertial effects into thermal and bulk inertia effects depends on the frame in which it is performed. While this may seem undesirable, it is the only form that smoothly transitions to the well-known nonrelativistic expression for small values of γ .

The electric field is hence expressed as

$$\vec{E} + \langle \vec{v} \rangle \times \vec{B} = \frac{1}{qn} \nabla \cdot \mathbf{P} + \frac{m}{q} \left(\frac{\partial}{\partial t} \langle \vec{u} \rangle + \langle \vec{v} \rangle \cdot \nabla \langle \vec{u} \rangle \right), \quad (16)$$

which is formally nearly identical to Eq. (2).

In this study, we will numerically evaluate all terms in Eq. (16). For simplicity, we will restrict the analysis to elec-

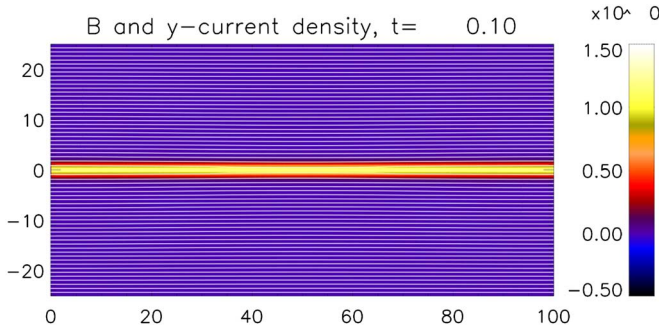


FIG. 1. (Color online) Magnetic field lines and y component of the current density at the beginning of the simulations. The figure shows the small, imposed, initial perturbation to the relativistic Harris equilibrium.

trons ($q=-e$). Since we will not investigate phase-space quantities, we will also drop the bracket indicating averaging for ease of writing.

III. MODEL AND INITIAL CONDITIONS

The simulations initiate from relativistic Harris sheet equilibrium¹⁵ with a small perturbation, which introduces an X-point topology. The magnetic field is normalized to its asymptotic value B_0 , the length scale is the nonrelativistic skin depth c/ω_e , and the time scale is an inverse, nonrelativistic, electron (or positron) cyclotron frequency. All other units are derived from this basic set.

The simulated system is 2.5 dimensional with simulation box dimensions of $L_x=100$ and $L_z=50$. The initial sheet thickness is $\lambda=1$. Positron and electron temperatures are equal, and the drift velocities in the current direction fulfill $v_{ey}=-v_{py}$. These conditions imply the selection of the frame where electrons and positron densities are equal, and where no large-scale charge separation exists. This choice is for convenience; in principle, the analysis could be performed in an arbitrary frame of reference.

We perform a total of six calculations: We perform two calculations each based on ratios of (nonrelativistic) plasma-to-cyclotron frequencies of $\omega_e/\Omega_e=2$, $\omega_e/\Omega_e=1$, $\omega_e/\Omega_e=0.5$, corresponding to values of the electron temperature in units of the electron rest energy of $T/mc^2=1/16$, $T/mc^2=1/4$, and $T/mc^2=1$.

The first set of calculations uses the perturbed relativistic Harris equilibrium as initial conditions, whereas the second set of calculations adds an initially constant guide magnetic field

$$B_{y0} = 1.5$$

to the setup. Magnetic field lines and the current density of the initial condition are displayed in Fig. 1. We point out that the addition of the guide magnetic field does not install a rotation of the geometry. Instead, the guide magnetic field changes the angle between the asymptotic magnetic fields at $|z|=z_{\max}$. Therefore, the orientation and frame chosen for the analysis are preferred as they permit the easiest approach to the analysis.

The simulations are performed using a fully relativistic version of our particle-in-cell code.² Additional diagnostics

TABLE I. Values of initial temperatures and guide magnetic fields for all of the simulations in this study.

Electron temperature/Guide magnetic field	$B_{y0}=0$	$B_{y0}=1.5$
$T/mc^2=1/16$	Run 1	Run 2
$T/mc^2=1/4$	Run 3	Run 4
$T/mc^2=1$	Run 5	Run 6

was developed for the purpose of the present studies. For each calculation, approximately 8×10^8 particles are moved on a grid of $n_x=800$ and $n_z=400$ cells. Boundaries in the x direction are periodic, and particles are specularly reflected at $|z|=z_{\max}$. Table I summarizes the parameters for each of the six runs. Time steps range from $\omega_e dt=0.1$ for the less relativistic simulations to $\omega_e dt=0.025$ for the runs with $\omega_e/\Omega_e=0.5$.

IV. EVOLUTION OVERVIEW

All six simulations exhibit the onset and evolution of one or more reconnection sites. As an example, Fig. 2 displays the magnetic field for run 4 for a set of times. The

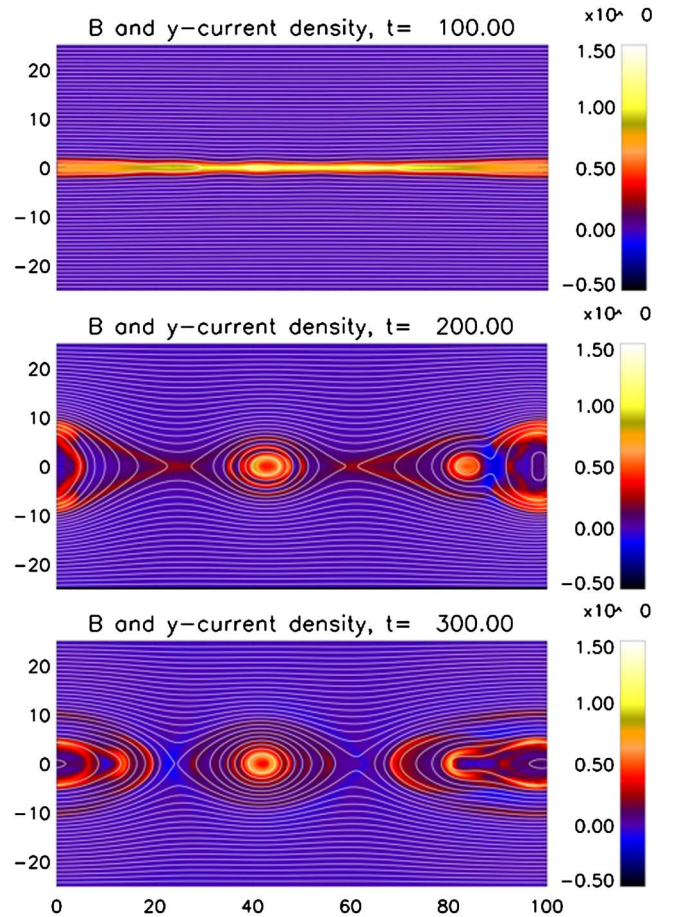


FIG. 2. (Color online) Magnetic field and current density j_y for run 4 for a set of times. The initial set of smaller islands rapidly coalesces to form a much smaller set of larger islands, which, however, reconnect at a considerably slower rate.

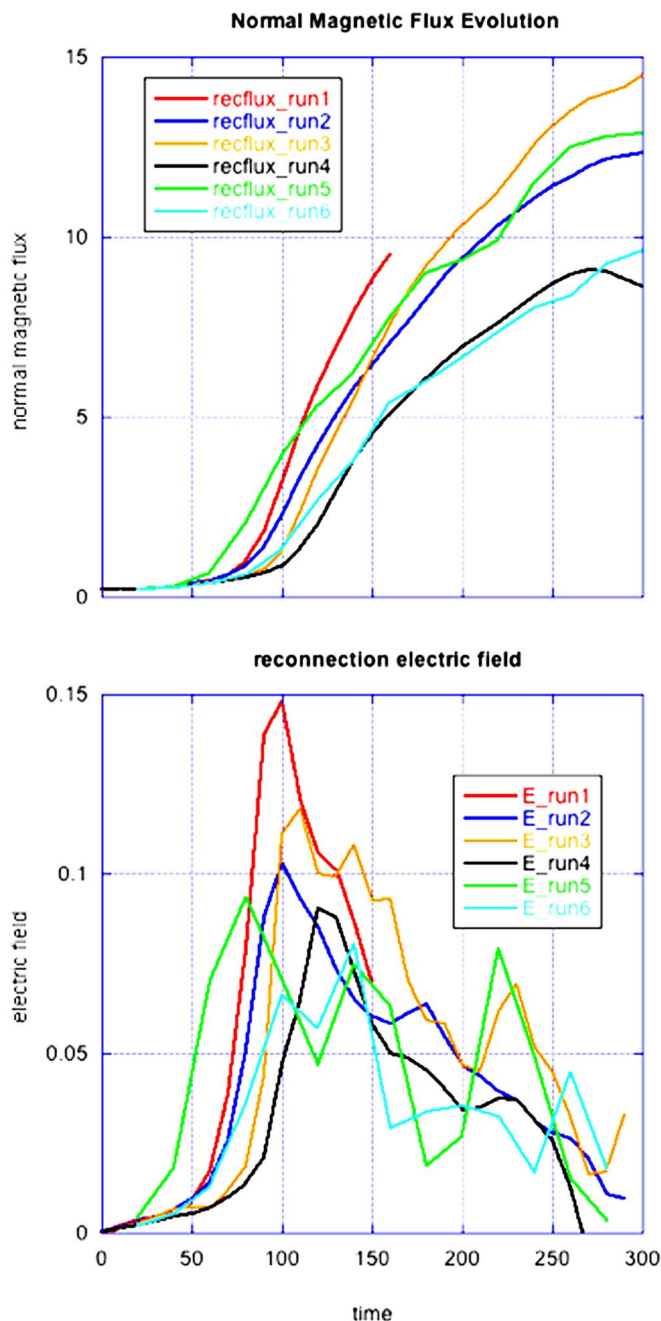


FIG. 3. (Color online) Time evolution of the magnetic flux normal to the x axis and of the reconnection electric field for all runs. Two clear trends are evident: Runs with more relativistic particles tend to evolve slower than those with fewer relativistic systems, and runs with a guide field reconnect slower than those without.

initial set of smaller islands rapidly coalesces to form much smaller sets of larger islands, which, however, reconnect at a considerably slower rate.

Time evolutions of the integrated magnetic flux along the x axis and of the reconnection electric field are shown in Fig. 3. The figure shows two clear trends: Runs with more relativistic particles tend to evolve slower than those with fewer relativistic computations (when the electric field is measured by the product of nonrelativistic Alfvén speed and magnetic field), and runs with a guide field reconnect slower than those without. The latter phenomenon is well

known,^{18,25} and due to the lower compressibility effect of the guide magnetic field. The effects of electron temperature have been seen before,^{18,21} and are likely due to the higher effective inertia of relativistic compared to nonrelativistic particles. The net effect is a reduction of the effective Alfvén speed, which reduces the overall reconnection rate. In fact, it is easily seen that the reconnection electric field, if multiplied by the square root of the average γ in the inflow region, is roughly identical for each of the two run groups with and without a guide magnetic field.

An overview of the degree of relativity for each run is shown in Fig. 4. The figure displays, for each run, the average value of γ for one time of the simulation, including that in the inflow region. There are a few noteworthy features. First, it is apparent that peak values of γ , indicative of larger average acceleration, occur typically for runs without a guide field. This difference is a consequence of the overall larger reconnection electric fields in runs without guide magnetic fields.

An additional difference stands out when comparing the panels for antiparallel reconnection with those for guide-field reconnection. While antiparallel reconnection appears to produce the highest values of γ inside magnetic islands, guide field reconnection produces very large enhancement of γ also at the X points. This point is emphasized in Fig. 5, which displays the magnetic field and current densities for the two most relativistic runs. Comparing the lower panels of Fig. 4 with the panels of Fig. 5 demonstrates that X points do not appear to be a major producer of higher energy particles for antiparallel reconnection, whereas they clearly are for run 6. This observation suggests that, in antiparallel reconnection, betatron-type acceleration at the magnetic pileup regions around the magnetic islands may be a major contributor to high-energy particles. For guide field reconnection, on the other hand, acceleration appears to occur primarily at the X point, and accelerated particles may be subsequently trapped inside a growing magnetic island. This result suggests that particle acceleration may play a more important role in the inner diffusion region of guide field magnetic reconnection. In turn, this could imply that bulk inertial effects may play a role. We will look at this question in the following section.

V. COMPOSITION OF THE RECONNECTION ELECTRIC FIELD

As recent investigations have shown that thermal inertia dominates the reconnection electric field in the inner diffusion region regardless of the presence of a guide magnetic field, the question arises whether this result extends to relativistic plasma also. A first hint at the results to come was already seen in Fig. 4, which indicated strong particle acceleration at the X point for guide-field reconnection, but not for antiparallel merging.

As a first step to studying the reconnection electric field, we will, for electrons, decompose the y component of Eq. (16) into its constituents. Figure 6 shows the results of executing this for run 6, at time $t=140$. The top left panel shows the convection electric field component. The panel

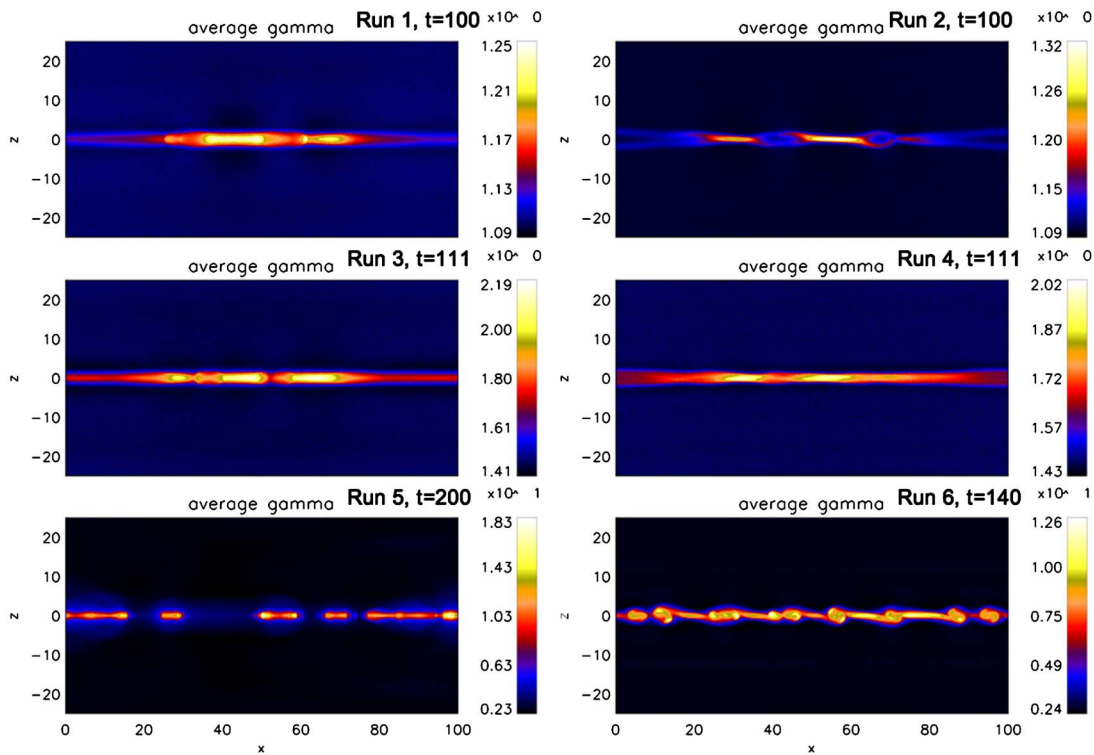


FIG. 4. (Color online) Average value of γ for one time of each of the simulations.

indicates enhancements around the inflow and outflow region of each X point, and negative values where magnetic islands expand in the z direction. This electric field term vanishes at each X point (see Fig. 5 for comparison).

The lower left panel displays the third term in Eq. (16). This term describes the convective transport of momentum.

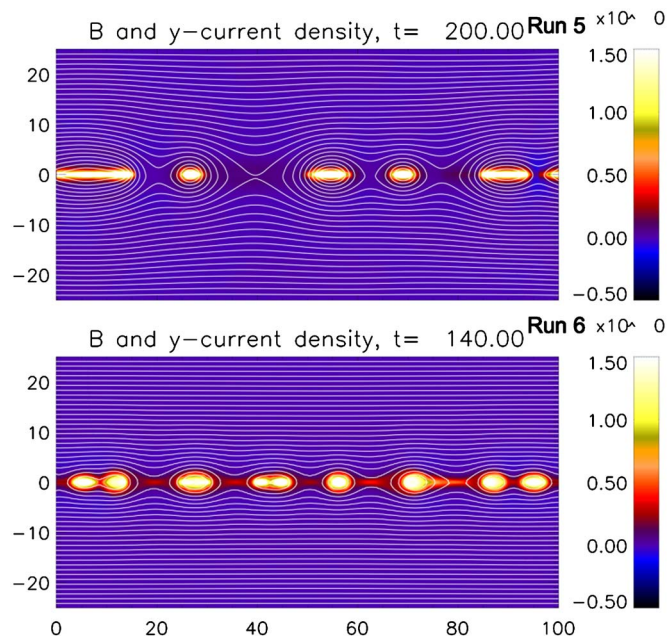


FIG. 5. (Color online) Comparison between the magnetic field and current densities for the two most relativistic runs. A comparison with Fig. 4 shows that X points are less likely to produce energetic particles in antiparallel reconnection than they are in guide field reconnection.

Since the average u_y typically peaks near the center of each reconnection site, the convective inertia term is also quite small at each X point. The top right panel, on the other hand, shows the thermal inertia, i.e., the electron pressure tensor-based term. As in the nonrelativistic simulations, the divergence of the pressure tensor is finite, and it appears to be a major contributor to the reconnection electric field. The final panel, however, shows a surprise. The time evolution of the bulk inertia, the fourth term in Eq. (16), apparently assumes a finite value at each X point as well. This result is entirely different from nonrelativistic calculations, and it deserves additional analysis (see below). At this point, there is evidence that bulk inertia may contribute significantly to the reconnection electric field, at least for guide-field reconnection, and fairly relativistic plasmas. In order to address this issue further, we pick, for each calculation, and for one representative time each, the most active X point. For each of these so-picked X points, we plot, along a segment of the X axis, all contributions to the reconnection electric field. The result is shown in Fig. 7.

The top row of panels depicts results for the calculations without guide fields, whereas the lower panels are for the three guide field runs. Each panel also shows the sum of all four constituent terms of E_y (light blue color), as well as the same electric field taken directly from the code (red). The panels show an excellent match between the electric field derived from the particle motion and the electric field resulting from the field solver in the code. This excellent match was achievable only by means of a rather large number of particles in each cell, which sufficiently limits numerical fluctuations.

electric field decomposition, run 6

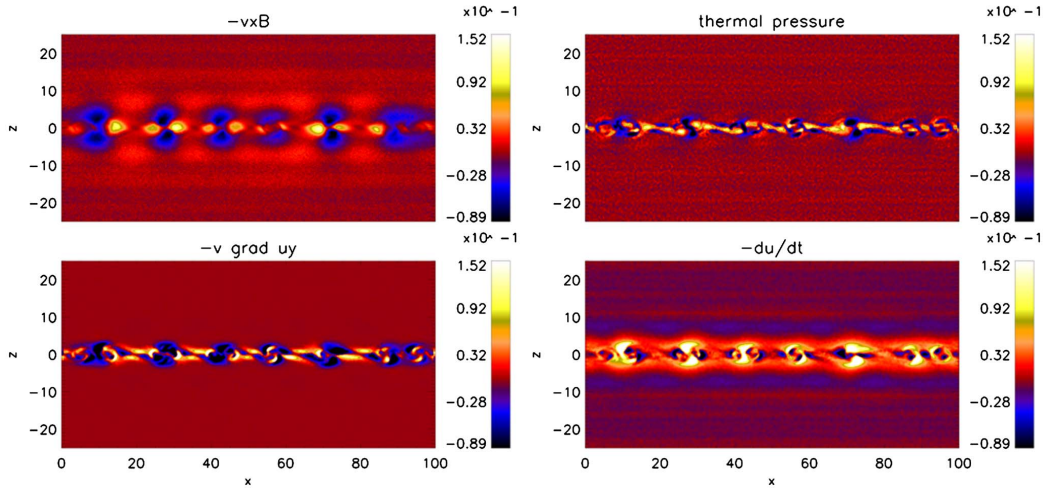


FIG. 6. (Color online) Decomposition of the y component of the electric field for run 6. Specifically, the top left panel shows the convection component, the top right panel shows the pressure tensor-derived electric field, the bottom left panel shows the convective element of the inertial terms, and the bottom right panel shows the Eulerian part of the inertial electric field. It is noteworthy that the time derivative of the bulk inertia (bottom right) contributes substantially to the total electric field at the X points.

Inspecting the top row of panels, we find consistently that the pressure tensor-based electric field by far dominates any other component in the central diffusion region. Large fluctuation may only be found at the edges of magnetic is-

lands for the highest value of the initial electron temperature, probably due to the effects of betatron-type acceleration. Near the X point, however, the system looks quite laminar with a smooth variation of the total electric field, as well as

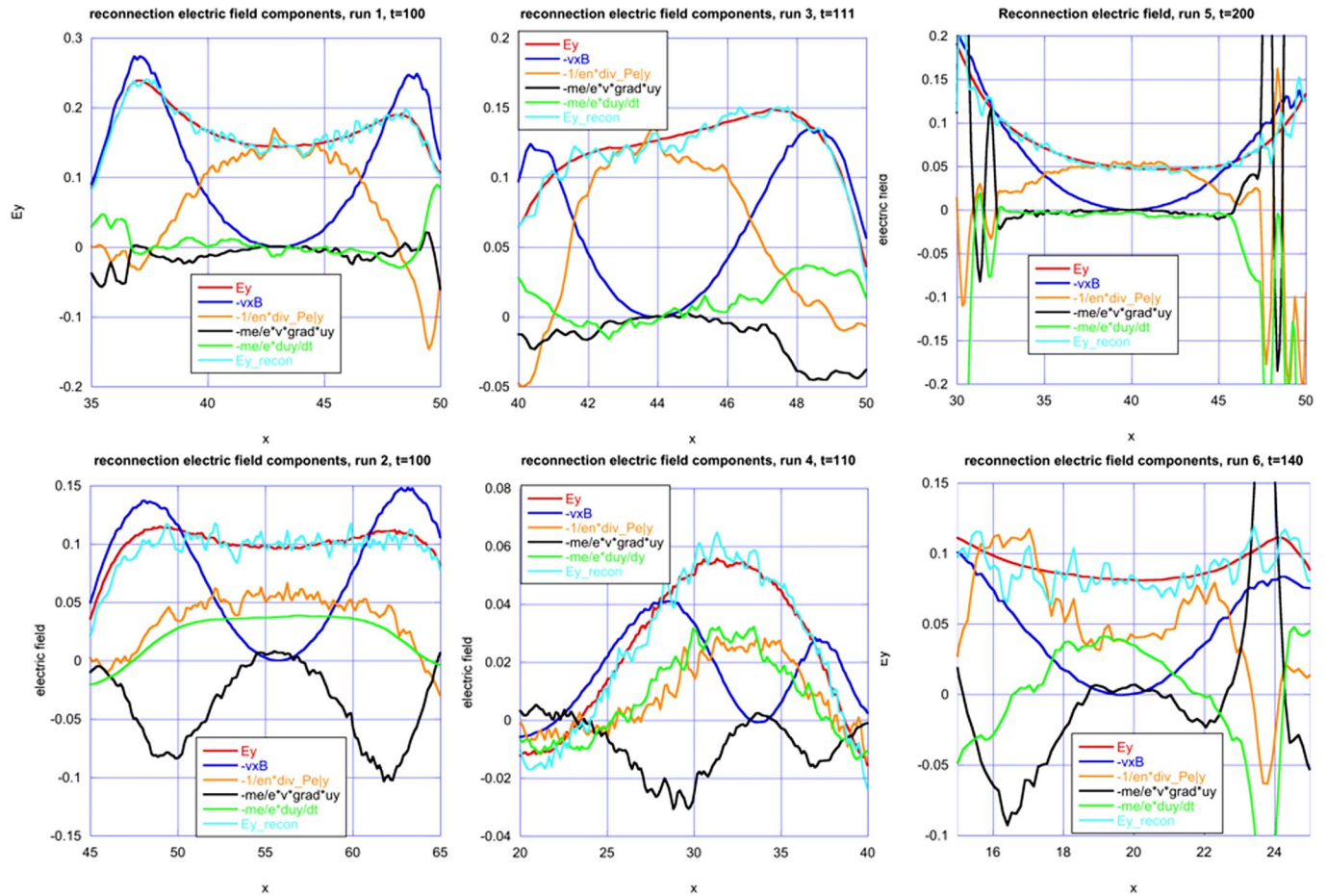


FIG. 7. (Color online) Plots along segments of the X axis of all components to the reconnection electric field near the dominant X point for each run.

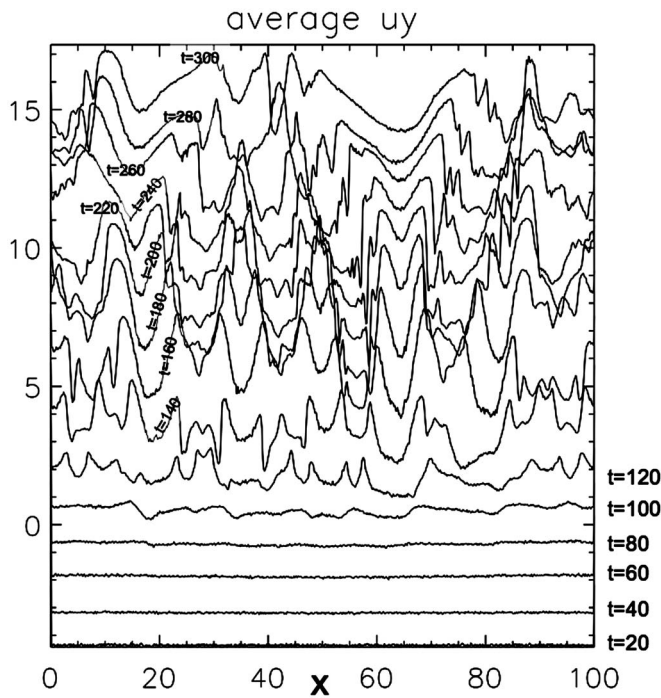


FIG. 8. Average momentum u_y along the x axis of the calculation for a set of simulation times of run 6. Shown are, from the bottom up, the traces of $u_y(x, z=0)$ for the electrons, for simulation times $t=20, 40, 60, 80, \dots, 300$. The traces are offset by a fixed value along the vertical (u_y) axis, i.e., plotted is $u_y(x, z=0, t) + du t$, where du is independent of t . Labels on the side or on the graphs indicate the respective times.

of all of its constituents. This result is identical to that found in classical reconnection,⁵ which shows that electron bounce motion-based dissipation will also apply in antiparallel reconnection in relativistic plasmas.

The bottom row of plots show that the physics changes in the presence of a guide field. For medium to moderate (runs 4 and 6) relativistic systems, we now find very strong contributions by inertial effects, in addition to those of the pressure tensor. A finite inertia effect is already present in the weakly relativistic calculation (run 2), where bulk inertia contributes approximately a third of the total electric field. For the more relativistic runs, bulk inertia effects roughly equal those of thermal inertia, and there is not much of a difference between runs 4 and 6. This result is substantially different from those of nonrelativistic calculations.

The effects of bulk inertia can, in principle, result from two effects. The first is a rapidly fluctuation current (or momentum) density, which, at any time, generates strong time derivatives of the average momentum. The second option is more laminar, and it involves a rapid but structured increase of the momentum density at the X point location. In order to investigate whether fluctuations or rapid growth are responsible, we plot for run 6 the average momentum u_y along the x axis of the calculation for a set of simulation times. The result is depicted in Fig. 8. The figure shows, from the bottom up, the traces of $u_y(x, z=0)$ for the electrons, for simulation times $t=20, 40, 60, 80, \dots, 300$. The relevant reconnection site is located approximately at $x=19.5$. Inspecting the time evolution, we note that a minimum in u_y begins to form at $t=100$, and develops rapidly until later than $t=160$. It

is easily seen that the time derivative of this minimum is sufficient to account for the magnitude of the inertia term, and the time change of u_y is essentially laminar.

Thus we find that bulk inertia, i.e., the net effect of an accelerated distribution, does indeed contribute significantly to the reconnection electric field. Why is this possible? There are two contributing factors. First, acceleration in the reconnection electric field is not current limited, i.e., further acceleration does not appreciably increase current density, while momentum density can increase without limits. This is not the case in a nonrelativistic plasma as momentum and current density are directly proportional to each other here.

The second factor is related to the fact that particles can spend relatively more time in the guide field reconnection region in a relativistic plasma. This implies that particles spend more time in the reconnection region than in nonrelativistic systems. This effect is most pronounced for guide field reconnection. Here, the Larmor radius

$$r_L = \gamma \frac{cm}{eB} \quad (17)$$

scales linearly with the Lorentz factor, whereas particle velocities are limited by the speed of light. Therefore, assuming that the reconnection region size is still given by the local electron Larmor radius,^{2,8} particles will spend, on average, more time in the diffusion region for more relativistic plasmas.

The same effect is considerably less pronounced for antiparallel reconnection. Here, the width of the diffusion region is given by the electron bounce width,^{4,5} which, for relativistic plasmas, assumes the form

$$L = \sqrt{\gamma \frac{cm}{eB}}, \quad (18)$$

where the magnetic field derivative can refer to $\partial B_x / \partial z$ or to $\partial B_z / \partial x$, depending on which scale is being considered. To first order, this expression increases only proportional to the square root of the Lorentz factor. Therefore, the time a particle spends inside the antiparallel diffusion region depends much more weakly on the average particle energy, and therefore the bulk inertia term should be considerably less important, as found in the present analysis.

VI. SUMMARY

In this paper, we presented a set of simulations of relativistic reconnection in pair plasmas. Similar to prior investigations,¹⁸⁻²² we chose pair plasmas as an investigative target due to their relevance in astrophysical plasmas, such as in pulsar winds.¹³⁻¹⁵ The objective of our investigations was to study how kinetic dissipation works in relativistic reconnection.

We studied two scenarios: antiparallel reconnection and guide-field reconnection, where the guide field strength exceeds that of the reconnection magnetic field components. Both systems were simulated for three levels of electron (positron) temperature, corresponding to three different lev-

els of the initial average value of the relativistic gamma factor. We saw strong similarities to nonrelativistic plasmas, but also some intriguing differences.

For the antiparallel simulations, we found that the pressure tensor-based dissipation, which was already identified in nonrelativistic reconnection,⁵⁻⁷ carries over to relativistic plasmas as well. The impact of bulk acceleration on the reconnection electric field was found to be small for the range of simulations investigated.

For guide field reconnection, the picture changed. Here we saw, with an increasing level of relativity, a strong role of bulk acceleration in the force balance, which involves the reconnection electric field. While the pressure tensor-based thermal dissipation persists, it supplies only approximately half of the force-balance if the plasma is relativistic enough. This is a deviation from nonrelativistic results,^{2,8-10} which show a strong dominance of the thermal dissipation mechanism.

We could motivate the behavioral difference between antiparallel and guide field reconnection by a set of simple estimates of particle residence time in the diffusion region. These estimates show that particles tend to spend disproportionately more time in the diffusion/acceleration region for guide field reconnection than in that for antiparallel reconnection if the plasma gets more relativistic. This enlarged residence time leads to relatively stronger bulk acceleration, and hence to a stronger role of the bulk inertia term.

We remark that the present investigation serves as just the first step in addressing the dissipation problem in relativistic plasmas. There are a number of open questions. For one, the role of the bulk inertia may, in principle, increase further for more relativistic plasmas, rendering the plasma behavior similar to that in the cold limit. If that were so, it would be in conflict with the notion that reconnection should be irreversible, i.e., that it should involve processes such as phase mixing or particle orbit chaos. A strong dependence on initial conditions within pressure tensor-based dissipation fits into this picture naturally, but bulk inertia does not. The resolution of this problem is a target for future investigations.

Lastly, we note that the present investigation does not

address the possibility of dissipation by wave modes with wave vectors aligned with the current direction. In nonrelativistic plasmas, it is agreed that antiparallel reconnection likely does not involve such modes, whereas there is some debate regarding guide field reconnection. This option deserves to be explored in relativistic plasmas as well.

ACKNOWLEDGMENTS

This research was supported by NASA's Heliophysics Theory Program (HPTP) and by NASA's MMS/SMART mission. The authors appreciate stimulating discussions with Karl Schindler, Masha Kuznetsova, Antonius Otto, and Jim Drake.

¹V. M. Vasyliunas, *Rev. Geophys. Space Phys.* **13**, 303 (1975).

²M. Hesse, *Phys. Plasmas* **13**, 122107 (2006).

³L. R. Lyons and D. C. Pridmore-Brown, *J. Geophys. Res.* **95**, 20903 (1990).

⁴R. Horiuchi and T. Sato, *Phys. Plasmas* **1**, 3587 (1994).

⁵M. Hesse, K. Schindler, J. Birn, and M. Kuznetsova, *Phys. Plasmas* **6**, 1781 (1999).

⁶P. L. Pritchett, *J. Geophys. Res.* **106**, 3783, DOI:10.1029/1999JA001006 (2001).

⁷M. Scholer, I. Sidorenko, C. H. Jaroschek, R. A. Treumann, and A. Zeiler, *Phys. Plasmas* **10**, 3521 (2003).

⁸M. Hesse, M. Kuznetsova, and J. Birn, *Phys. Plasmas* **11**, 5387 (2004).

⁹M. Swisdak, J. F. Drake, M. A. Shay, and J. G. McIlhargey, *J. Geophys. Res.* **110**, A05210, DOI:10.1029/2004JA010748 (2005).

¹⁰G. Lapenta, D. Krauss-Varban, H. Karimabadi, J. D. Huba, L. I. Rudakov, and P. Ricci, *Geophys. Res. Lett.* **33**, L10102, DOI:10.1029/2005GL025124 (2006).

¹¹T. di Matteo, *Mon. Not. R. Astron. Soc.* **299**, L15 (1998).

¹²H. Lesch and G. T. Birk, *Astrophys. J.* **499**, 167 (1998).

¹³F. V. Coroniti, *Astrophys. J.* **349**, 538 (1990).

¹⁴Y. Lyubarsky and J. G. Kirk, *Astrophys. J.* **547**, 437 (2001).

¹⁵J. G. Kirk and O. Skjæaasen, *Astrophys. J.* **591**, 366 (2003).

¹⁶G. Drenkhahn, *Astron. Astrophys.* **387**, 714 (2002).

¹⁷G. Drenkhahn and H. C. Spruit, *Astron. Astrophys.* **391**, 1141 (2002).

¹⁸N. Bessho and A. Bhattacharjee, *Phys. Plasmas* **14**, 056503 (2007).

¹⁹S. Zenitani and M. Hoshino, *Astrophys. J. Lett.* **562**, L63 (2001).

²⁰S. Zenitani and M. Hoshino, *Phys. Rev. Lett.* **95**, 095001 (2005).

²¹S. Zenitani and M. Hoshino, *Astrophys. J.* **670**, 702 (2007).

²²C. H. Jaroschek, R. A. Treumann, H. Lesch, and M. Scholer, *Phys. Plasmas* **11**, 1151 (2004).

²³A. H. Taub, *Phys. Rev.* **74**, 328 (1948).

²⁴T. P. Wright and G. R. Hadley, *Phys. Rev. A* **12**, 686 (1975).

²⁵J. D. Huba and L. I. Rudakov, *Phys. Plasmas* **9**, 4435 (2002).